ELSEVIER

Journal of Power Sources 102 (2001) 60–67

JOURNAL OF POWER SOURCES

www.elsevier.com/locate/jpowsour

Electrochemical performance of Ni-deposited graphite anodes for lithium secondary batteries

Lihong Shi, Qing Wang, Hong Li, Zhaoxiang Wang, Xuejie Huang, Liquan Chen*

Laboratory for Solid State Ionics, Institute of Physics, Chinese Academy of Sciences, P.O. Box 603, Beijing 100080, China

Received 05 June 2000; received in revised form 02 August 2000; accepted 22 March 2001

Abstract

A series of Ni-deposited natural graphite composite materials have been prepared by hydrothermal hydrogen reduction method. The size of the Ni bead is determined to be around 300 nm and most of the Ni beads are distributed on the edge planes of a graphite particle. The electrochemical performance of these composites has been studied as active anode material for lithium ion batteries. It is found that the composite materials have a higher discharge capacity than that of pure graphite electrode at high current density. The improved rate performance of the Ni-deposited graphite samples is attributed to the lower electron transfer resistance and the improvement of the electronic conductivity of the composite materials.

Keywords: Ni-deposited graphite; Electrochemical impedance spectroscopy (EIS); Lithium ion batteries

1. Introduction

Carbonaceous materials have been extensively studied as negative electrode in lithium ion batteries because Li ions can be intercalated into and deintercalated from these materials reversibly [1–11]. Graphite is a very important anode material for lithium ion batteries due to its high reversible capacity, flat voltage profile and low cost. However, the rate performance of graphite materials, especially those with flaky morphology, is not satisfactory for high power density batteries. Two factors at least limit the kinetic properties of the flaky graphite. One is the highly anisotropic property of the well-defined graphite [12–16]. Its conductivity in the *a*-axis direction is much higher than along the *c*-axis. It is known that most of the Li ions intercalate into the graphite lattice from the edge plane instead of from the basal plane. In practical electrodes composed of flaky graphite, most of the basal planes are tended to be parallel to the current collector and perpendicular to the mobile direction of the Li ions in the electrode. This geometric configuration comes to be the second limitation factor and is not beneficial to the insertion of Li ions at large current density. In addition, each graphite flake in an anode is covered with a layer of solid electrolyte interphase (SEI) after several charge and discharge cycles [17–22]. Consequently, the electronic conductivity of the electrode is reduced gradually. In order to solve these problems, some efforts have been taken to modify the graphite, such as coating the surface with a layer of hard carbon or superfine Ag powder as well as the addition of some metal fibers [23–28]. These modifications improve the rate performance of the carbon electrode significantly, especially for the Ag-deposited graphite. However, as 10% silver is required to achieve a better rate performance in a Ag-deposited graphite, this is not a very economical choice, especially for large-scale Li ion batteries used for electric vehicles.

Considering the above problems, Ni-deposited graphite composite materials were prepared and their electrochemical properties were studied in this work. Our attention was paid mainly to build up a correlation between the kinetic performance and the Ni content in the electrode material.

2. Experimental

2.1. Material preparation

$NiSO_4$, $(NH_4)_2SO_4$, $NH_3{\cdot}H_2O$ used in the study were commercial products and natural graphite (99.9%, 325 meshes) was obtained from Nanshu Carbon Company (Shandong, China). There have been several methods to deposit nickel on the graphite surface such as electrodeposition of $Ni(CO)_4$, chemical deposition. Hydrothermal deposition is superior to other methods because it is nontoxic, easy to operate and superfine particles can be obtained [29]. In this work, composite materials with different weight ratios

* Corresponding author. Fax: +86-10-826490501.
E-mail address: qchen@aphy02.iphy.ac.cn (L. Chen).

0378-7753/01/$ – see front matter
PII: S0378-7753(01)00773-X

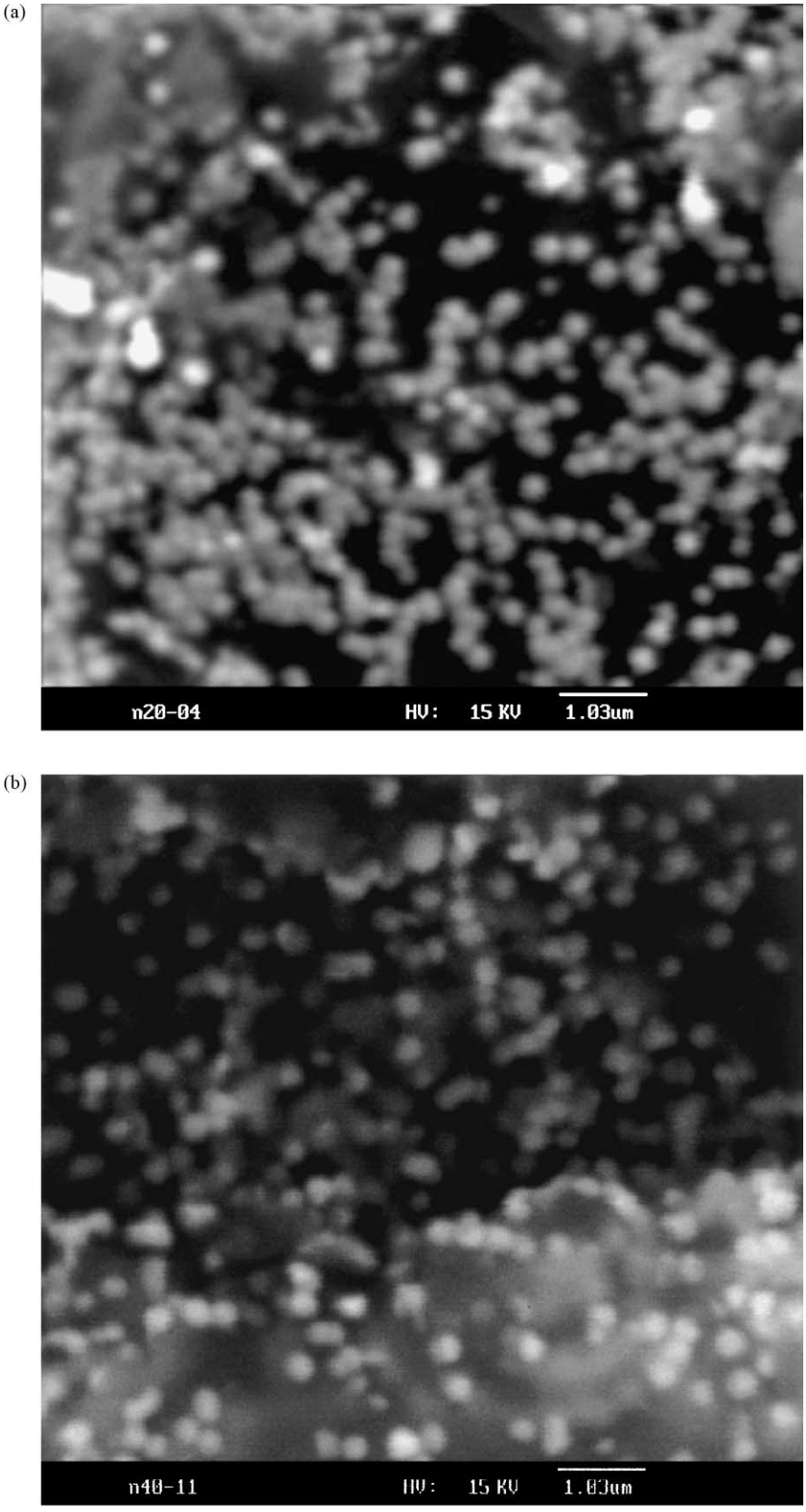

Fig. 1. The SEM images of NiG1 (a) and NiG3 (b) samples. (c) The X-ray patterns of Ni-deposited graphite. The diffraction peaks belonging to Ni have been specially notified.

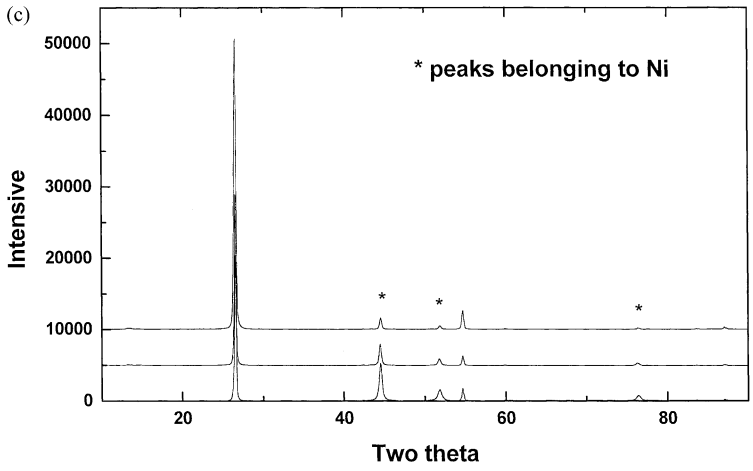

Fig. 1. (*Continued*).

of nickel to graphite were prepared by hydrothermal hydrogen reduction method [29] as follows:

$$\mathrm{Ni(NH_3)_nSO_4 + H_2 + C_{(graphite)}} \xrightarrow{\text{surface\_active\_agent}} \mathrm{Ni/C + (NH_4)_2SO_4 + (n-2)NH_3}, \quad (n \geq 2)$$

The above reaction was carried out in an autoclave by unceasingly stirring the sample at 150°C and at a high pressure of flowing H_2. After the reaction, the powder product was filtrated, rinsed and ultimately dried at 80°C for 12 h in vacuum. All the XRD peaks (Fig. 1c) of each sample belong to either metallic Ni or graphite. Chemical analysis shows that the weight percentages of Ni are 9, 27 and 38%, respectively, in NiG1, NiG2 and NiG3. The morphology of the samples was investigated with a Hitachi S-4200 scanning electronic microscope.

2.2. Fabrication of working electrode

The working electrodes were prepared by casting the slurries of active materials (92% w/w) and polyvinylidene fluoride (PVDF) (8% w/w) dissolved in cyclopentanone onto a copper foil. After that, the electrode sheet was dried at 120°C for 8 h in vacuum and then pressed between two stainless steel plates at 1 MPa pressure. Working electrodes with 0.81 cm^2 area were cut from the sheet and dried again at 120°C for 4 h in vacuum before the cell assembly.

2.3. Electrochemical testing

Two-electrode cells were constructed with Celgard® 2300 as separator, 1 M $LiPF_6$ in EC-DEC (1:1 v/v) as electrolyte, pure Li foil as the counter electrode and the composite material described above as the working electrode. They were assembled into a cell in an argon-filled glove box. The cells were charged at a current density of 0.1 mA/cm^2 and discharged at different current densities when the high rate discharge performance was examined.

A three-electrode glass cell was used for measuring the electrochemical impedance spectroscopy (EIS) [25,30–32]. Li metal was used as both reference and counter electrodes. The impedance spectra were recorded in a frequency range from 10 kHz to 0.01 Hz by a Solartron 1170 frequency response analyzer coupled with a 1186 electrochemical interface. Before each EIS measurement, the cell was discharged to a preset voltage and then kept at that voltage until the current decays to <4 μA.

3. Results and discussion

3.1. The distribution of ultra fine Ni particles on graphite

Fig. 1a and b show typical SEM images of NiG1 and NiG3 samples. It can be seen that the Ni particles with a diameter around 300 nm distribute randomly on the graphite surface. A common feature of all the samples is that the particle size of Ni is independent of its content and its position on the graphite surface. This means that the deposition is a homogenous nucleation process. However, the distribution of Ni particles on graphite surface is not uniform as shown in Fig. 2a. Most of the Ni particles are distributed on the edge plane of the graphite particle. The weight ratio Ni:C is 3:1 on the edge plane of the graphite particle but only 1:3 on the basal plane based on the energy dispersion analysis of X-ray (EDAX) results shown in Fig. 2b. This preferential distribution might be attributed to the high anisotropy in chemical activity of natural graphite.

3.2. Discharge and charge performances

It can be seen in Fig. 3 that the charge and discharge curves of Ni-deposited graphite samples show profiles similar to that of natural graphite [1–7]. This implies that no side reaction was observed except for the intercalation and deintercalation of Li in the Ni-deposited graphite.

As metallic Ni is electrochemically inactive in this case, it is obvious that the addition of Ni will decrease the specific capacity of the electrode material. However, this disadvantage is compensated by the excellent rate performance of this material as shown in the following.

3.3. Rate performance

In this work, the discharge capacity ratio is defined as the ratio of the discharge capacity of a material at a certain current density to that at the current density of 0.1 mA/cm^2 for the same material. The relationship between the discharge capacity and discharge current density for Ni-deposited graphite samples is shown in Fig. 4. Due to the inactivity of metallic Ni, the reversible capacity of Ni-deposited graphite is obviously lower than that of pure graphite at small current densities from 0.1 to 0.3 mA/cm^2. The capacity ratio of the material increases with the Ni content in the sample before the current density reaches 0.7 mA/cm^2. This is due to the improvement of the electrical conduction to the electrode material as a result of the existence of the Ni beads on the graphite. However, the capacity ratio shows different features when the Ni content reaches about 27%. When the current is below 0.6 mA/cm^2, the ratio continues to increase with the Ni content. But when the current is above 0.6 mA/cm^2, the ratio decreases with the Ni content. A reasonable explanation to this phenomenon is that the Ni beads partially block the intercalation and deintercalation of the Li ions. When the current density is low, the Li ions have enough time to bypass the Ni beads and the capacity ratio will not decrease significantly. Nevertheless, the Li ions will be severely blocked when the current density is very high. Therefore, we propose that 27% of Ni on the graphite surface is the optimal content that can improve the rate performance but will not sacrifice other performances of the electrode material.

3.4. EIS results

The improvement of the rate performance should be related to the increase of the conductivity and the variation of kinetic parameters in the electrode process.

The electrochemical impedance spectroscopic measurements were carried out at various potentials for NiG2 and NiG3 and pure graphite, respectively. The spectra in the form of Nyquist plots were fitted with the software Zview of Solartron and the equivalent circuits employed here were shown in Fig. 5. The exchange current density i^0 can be calculated from the fitting results according to the equation

$$i^0 = \frac{RT}{FR_{ct}} \quad (1)$$

where R_{ct} is the charge transfer resistance, R and F are the gas and Faraday constants, respectively. The calculated

(a)

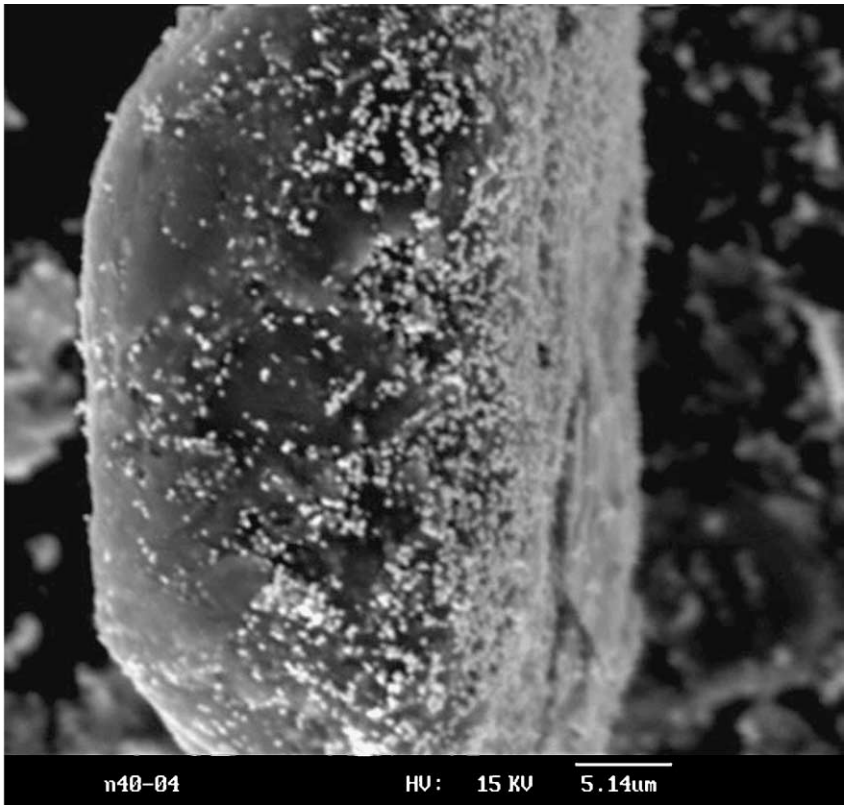

Fig. 2. (a) The distribution of Ni on a graphite particle by SEM. It is seen that the Ni beads prefer to stand at the edge planes of the particle. (b) Typical EDAX spectra at the edge (upper) and at the basal planes (lower) of a Ni-deposited graphite particle.

(b)

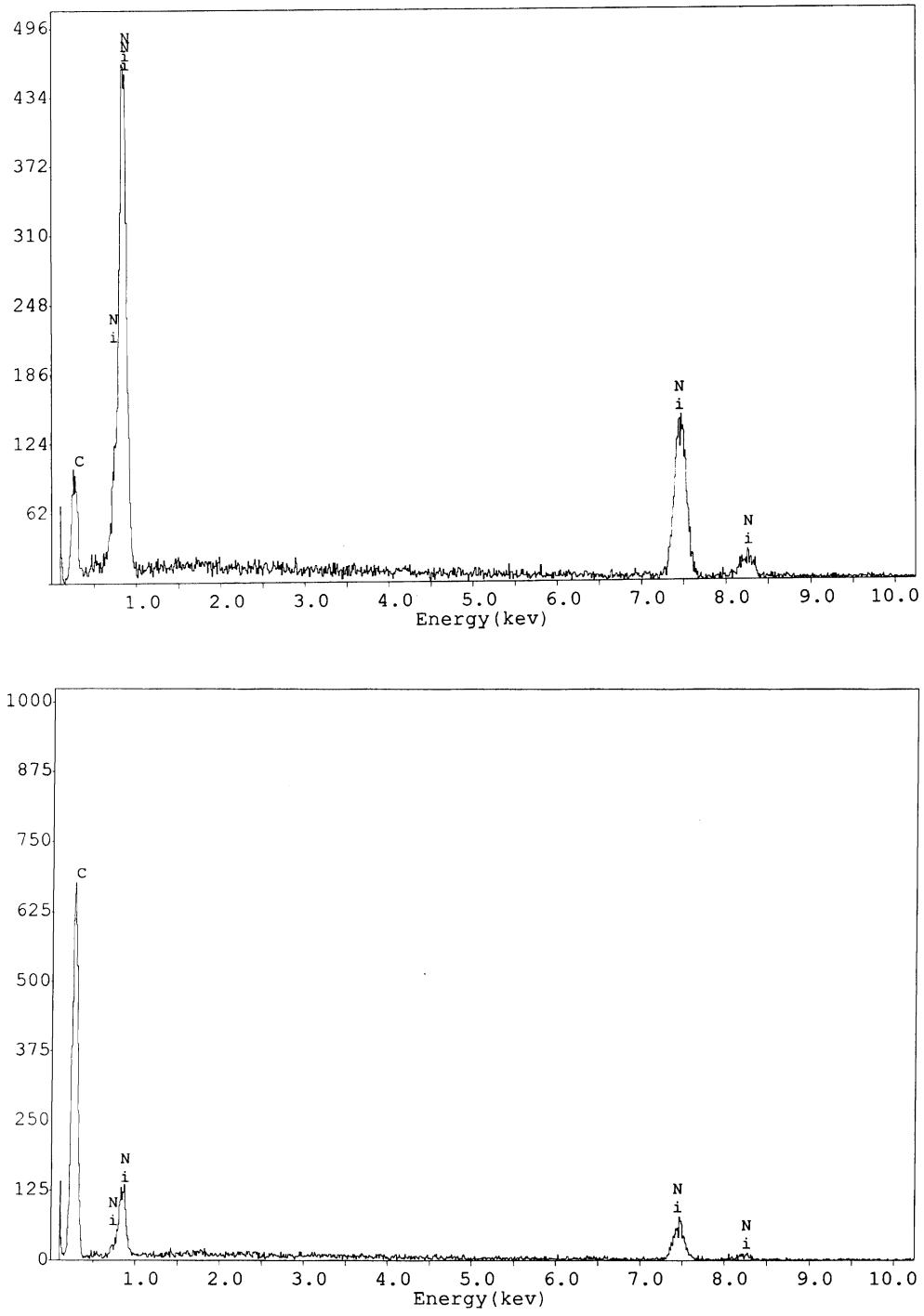

Fig. 2. (*Continued*).

exchange current density and the fitted value of the electric resistance of SEI film divided by double layer capacitance at different equilibrium potentials were shown in Figs. 6 and 7, respectively. It is obvious that the exchange current density of NiG3 and NiG2 electrodes are much larger than that of pure graphite at lower potentials where Li ions intercalation occurs. Therefore, Ni-deposition is beneficial to charge transfer process.

Since a SEI film generally covers the surface of an anode in lithium secondary batteries, it is interesting to know the influence of Ni particles deposited on the surface of graphite in the SEI film. The film resistance (R_f) for these samples shows complicated variation as shown in Figs. 6 and 7. Under the same potential, the R_f of pure graphite is higher than in Ni-deposited samples. It is believed that some Ni particles might stud in the SEI film, so the conductivity of

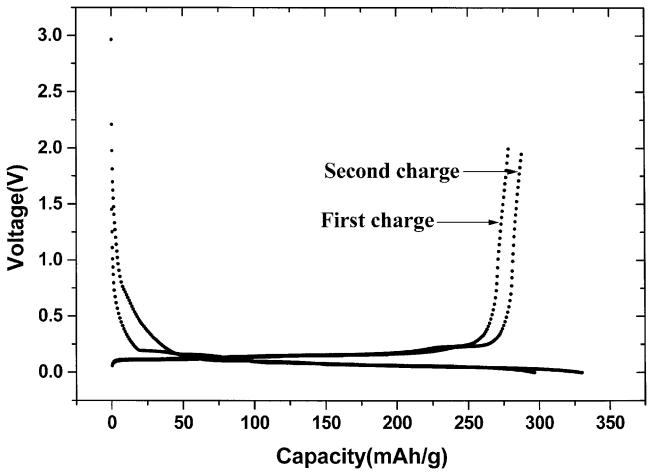

Fig. 3. The discharge and charge curves of a cell, with NiG1 as the working electrode. The current density is 0.1 mA/cm^2 for discharge and recharge.

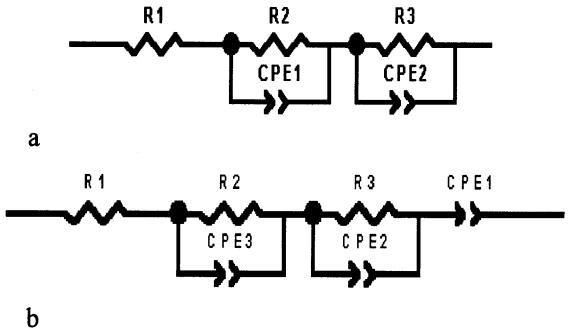

Fig. 5. The equivalent circuits employed to fit the Nyquist plots of electrochemical impedance spectra at different equilibrium potentials: (a) above 1.2 V; (b) at and below 1.2 V.

the SEI film is increased. Furthermore, since the size of Ni particles is 250 nm and the thickness of SEI film is generally only 2–4 nm [17,20–22], Ni particles might extrude the SEI film. It is beneficial to keep a good electronic contact for each graphite particle that was covered by the SEI film during electrochemical cycles.

The EIS results show that the exchange current density is the highest in NiG3 (graphite containing 38% deposited Ni). However, its discharge capacity is lower than that of NiG2 throughout the discharge current densities applied in this work as shown in Fig. 4.

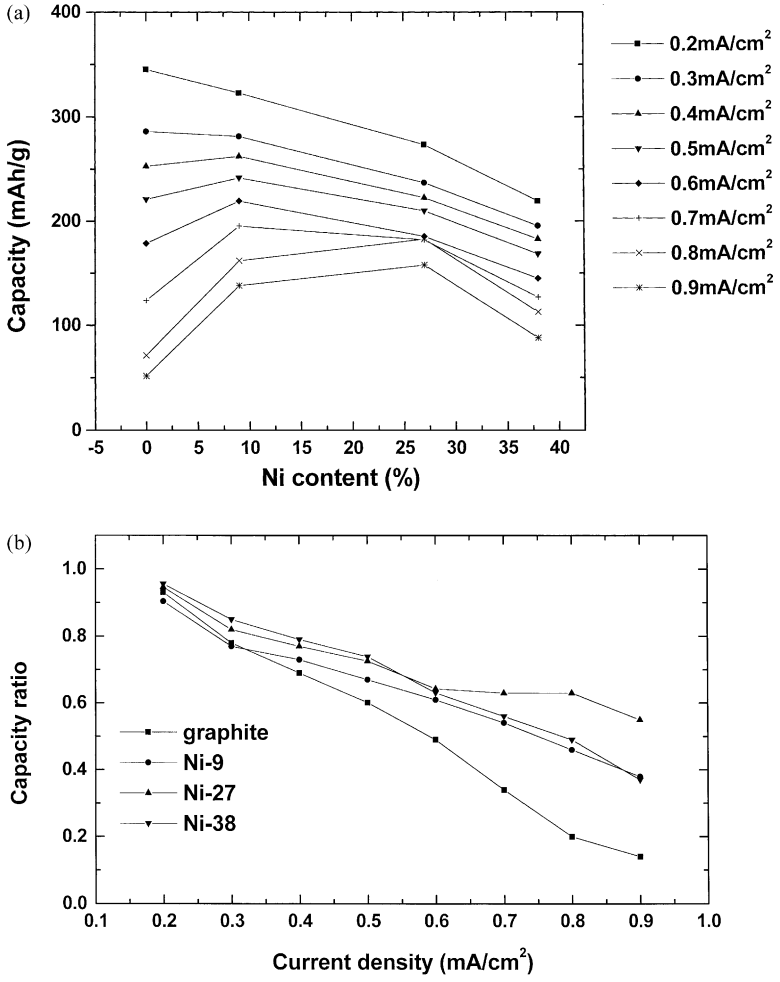

Fig. 4. The rate performance for series of NiGx materials used as anode active materials for lithium ion batteries: (a) the capacity ratio vs. Ni content; (b) the capacity vs. the current density.

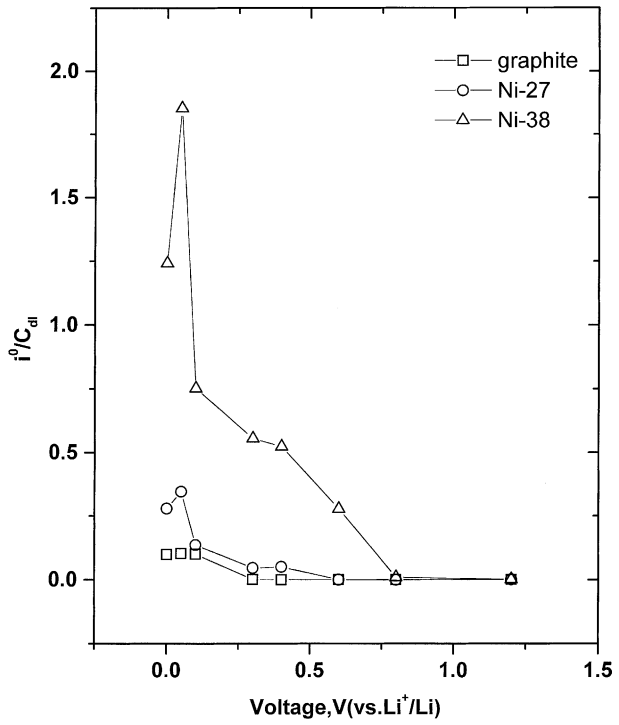

Fig. 6. The calculated exchange current density divided by double layer capacitance at different equilibrium potentials.

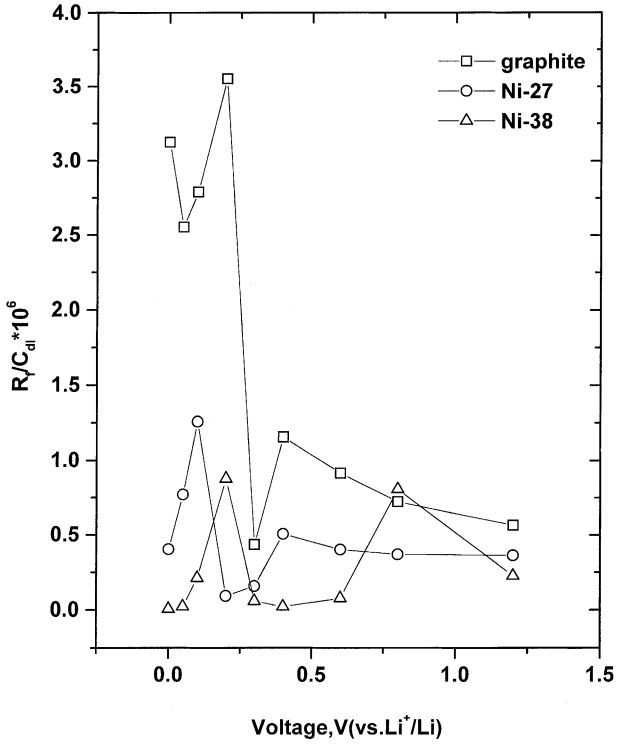

Fig. 7. The calculated electric resistance divided by capacitance of the double layer at different equilibrium potentials.

4. Conclusions

Ni-deposited natural graphite composite materials have been prepared using hydrothermal hydrogen reduction method. The particle size of Ni is around 300 nm and is independent of the Ni content. The Ni particles are preferentially distributed on the edge planes. The rate performance of Ni-deposited graphite as anode for lithium ion cells is improved. This may be due to the decrease of charge transfer resistance and the SEI film resistance as well as to the increase of the electronic conductivity.

Acknowledgements

Authors are grateful to Dr. Chendong Bai for his help in preparing the Ni-deposited graphite samples. This work was financially supported by NSFC (contract no. 59972041) and National 863 Key Program (contract no. 715-004-0280).

References

[1] M. Mohri, N. Yanagisawa, Y. Tajima, H. Tanaka, T. Mitate, S. Nakajima, M. Yoshida, Y. Yoshimo, T. Suzuki, H. Wade, J. Power Sources 26 (1989) 545.
[2] J.R. Dahn, A.K. Sligh, H. Shi, B.M. Way, W.J. Weydanz, J.N. Reimers, Q. Zhang, U. Von Sacken, in: G. Pistoia (Ed.), Lithium Batteries — New Materials, Developments and Perspectives, Elsevier, New York, 1994, p. 1.
[3] J.M. Tarascon, D. Guyomard, J. Electrochem. Soc. 138 (1991) 2864.
[4] J.R. Dahn, R. Fong, M.J. Spoon, Phys. Rev. B 42 (1990) 6424.
[5] D. Guyomard, J.M. Tarascon, J. Electrochem. Soc. 139 (1992) 937.
[6] M. Arakawa, J.I. Yamaki, J. Electroanal. Chem. 219 (1987) 273.
[7] J.R. Dahn, Phys. Rev. B 44 (1991) 9170.
[8] N. Takami, A. Satoh, M. Hara, T. Ohsaki, J. Electrochem. Soc. 142 (1995) 371.
[9] D. Aurbach, Y. Ein-Eli, B. Markovsky, A. Zaban, A. Schechter, S. Luski, Y. Carmeli, H. Yamin, in: S. Megahed, B. Barnett, L. Xie (Eds.), Proceedings of Symposium on Rechargeable Lithium and Lithium-Ion Batteries, Vols. 94–28, Battery Division, The Electrochemical Society, 1995, p. 26.
[10] T. Takamura, H. Awano, T. Ura, K. Sumiya, J. Power Sources 68 (1997) 114.
[11] T. Ohzuku, Y. Iwakoshi, K. Sawai, J. Electrochem. Soc. 140 (1993) 2490.
[12] E. Barendrecht, J. Appl. Electrochem. 20 (1990) 175.
[13] L.A. Girifalco, R.A. Lad, J. Chem. Phys. 25 (1950) 693.
[14] H. Shi, J. Barker, M.Y. Saidi, R. Koksbang, J. Electrochem. Soc. 143 (1996) 11.
[15] N. Greenwood, A. Earnshow, Chemistry of the Elements, Pergamon Press, New York, 1984, p. 296.
[16] R.W. Lynch, H.G. Drickamer, J. Chem. Phys. 44 (1996) 181.
[17] E. Peled, D. Golodenitsky, G. Ardel, C. Menachew, D. Bartow, V. Eshkenasy, in: D.H. Doughty, B. Vyas, T. Takamara, J.R. Huff (Eds.), Materials for Electrochemical Energy Storage and Conversion — Batteries, Capacitors and Fuel Cells, Material Research Society Symposium Proceedings, No. 393, Material Research Society, Pittsburgh, NJ, 1995, p. 209.
[18] D. Aurbach, Y. Ein-Ely, J. Electrochem. Soc. 142 (1995) 1746.

[19] D. Aubach, Y. Ein-Eli, B. Markovsky, A. Zaban, S. Luski, Y. Carmeli, H. Yamin, J. Electrochem. Soc. 142 (1995) 2882.
[20] D. Aurbach, Y. Ein-Eli, O. Chusidl, Y. Carmeli, M. Babai, H. Yamnin, J. Electrochem. Soc. 141 (1994) 603.
[21] E. Peled, J. Electrochem. Soc. 126 (1979) 2047.
[22] E. Peled, Rechargeable lithium and Lithium ion batteries, in: S. Megahed, B.M. Barnett, L. Xie (Eds.), The Electrochemical Society Softbound Series PV 94-28, The Electrochemical Society Inc., Pennington, NJ, 1995, pp. 1–15.
[23] C. Menachem, E. Peled, L. Brstein, Y. Rosenberg, J. Power sources 68 (1997) 277–282.
[24] T. Takamura, K. Sumiya, J. Power Sources 81/82 (1999) 368–372.
[25] E. Peled, G. Manchem, D. Bar-Tow, A. Melman, J. Electrochem. Soc. 143 (1996) L4.
[26] C. Menachem, E. Peled, L. Burastein, Y. Rosenberg, J. Power Sources 68 (1997) 277.
[27] W.H. Qiu, G. Lu, S.G. Wu, Q.G. Liu, Chin. J. Power Sources 23 (1999) 1.
[28] H. Honbo, S. Takeuchi, H. Momose, K. Nishimura, T. Horiba, Denki Kagaku 66 (9) (1998) 939–944.
[29] L. Huangzhen, M. Minghua, Zh. Rongyuan, Eng. Chem. Metall. 17 (2) (1996) 111.
[30] E. Peled, J. Electrochem. Soc. 126 (1979) 2047.
[31] M.D. Levi, D. Aurbach, J. Phys. Chem. B 101 (1997) 4630–4640.
[32] E. Peled, D. Bar-Tow, A. Melman, E. Gerenrot, Y. Lavi, Lithium Batteries, N. Daddapaneni, A.R. Langret (Eds.), The Electrochemical Society Proceedings Seenes, PV 94-4, Pennington, NJ, 1994, p. 177.